



Assessing the Statistical Uniqueness of the Younger Dryas: A Robust Multivariate Analysis

Henry Nye¹ and Alan Condron²

¹Department of Mathematics and Statistics, Haverford College, PA 19041

²Geology and Geophysics, Woods Hole Oceanographic Institution, MA 02543

Correspondence: Henry Nye (hnye@haverford.edu), Alan Condron (acondron@whoi.edu)

Abstract. During the last glacial period (c. 120-11 kyr BP), dramatic temperature swings, known as Dansgaard-Oeschger (D-O) events, are clearly manifest in high resolution oxygen isotope records from the Greenland ice sheet. Although variability in the Atlantic Meridional Overturning Circulation (AMOC) is often invoked, a unified explanation for what caused these ‘sawtooth shaped’ climate patterns has yet to be accepted. Of particular interest is the most recent D-O shaped climate pattern that occurred from ~14,600 to 11,500 years ago - the Bølling/Allerød (BA) warm interstadial and the subsequent Younger Dryas (YD) cold stadial. Unlike earlier D-O stadials, the YD is frequently considered a unique event, potentially resulting from a rerouting and/or flood of glacial meltwater into the North Atlantic, a meteorite impact, or a volcanic eruption. Yet, these mechanisms are seldom considered as the cause of the earlier stadials. Using a robust multivariate outlier detection scheme - a novel approach for traditional paleoclimate research - we show that the pattern of climate change during the BA/YD is not statistically different from the other D-O events in the Greenland record, and that it should not be considered unique when investigating the drivers of abrupt climate change. Our results thus raise important questions about the ability of glacial meltwater input and other ‘one off’ events to trigger abrupt, centennial-to-millennial length, changes in climate.

1 Introduction

First noted in 1985 by Willi Dansgaard as “violent oscillations” in Greenland’s DYE-3 and Camp Century oxygen isotope ($\delta^{18}\text{O}$) records, Dansgaard-Oeschger (D-O) events are now well known examples of abrupt climate change during the last glacial period (c. 120-11 kya BP) (see Figure 1) (Dansgaard, 1985). These events are characterized by abrupt warmings of ~ 8-16° C, a subsequent centennial-to-millennial length period of relative warmth (i.e. an interstadial), followed by a gradual, and sometimes abrupt, shift to cooler (stadial) conditions. Since their discovery three and a half decades ago, countless mechanisms have been proposed to explain D-O cycles (see Li and Born (2019) for a review). Although most hypotheses invoke changes in ocean heat transport as a consequence of variations in the strength of the Atlantic Meridional Overturning Circulation (AMOC) (Broecker et al., 1985), it remains poorly understood as to what would have caused the overturning cell to undergo such large



and rapid changes (Lohmann and Ditlevsen, 2019). While variations in atmospheric circulation, sea ice extent, and ice shelf formation/collapse have all being hypothesized as triggers, a unifying theory has yet to emerge (Lohmann and Ditlevsen, 2018).
25 Given that D-O events provide compelling evidence that the Earth's climate can rapidly switch from one state to another, it is imperative that we determine the causes of this variability if we are to accurately predict future climate.

In the original work of Dansgaard (Dansgaard, 1985), the most recent saw-tooth shaped interstadial stadial sequence of climate change since 120,000 years ago, associated with the Bølling-Allerød warming and Younger Dryas stadial (abbreviated here to BA/YD) from ~14,600 to 11,700 years BP was labeled as D-O event 1 (Figure 1). Since then, however, a growing body
30 of geological evidence attributing the Younger Dryas cooling to a glacial outburst flood and/or a change in glacial meltwater drainage patterns to the ocean (Broecker et al., 1989; Clark et al., 2001; Keigwin et al., 2018) has often led to this episode being treated as a unique event, rather than as one of the D-O stadials (Li and Born, 2019). Evidence that the YD cooling also might have coincided with “one-time” events such as a meteorite impact (Firestone et al., 2007) and/or a large volcanic eruption (Baldini et al., 2018) capable of ‘blocking out’ incoming solar radiation has helped bolster this notion. In this paper,
35 we use a multivariate outlier method to re-examine the extent to which the BA/YD should be considered ‘unique’ in the context of the other D-O events. The motivation for this study derives from the remarkable similarities in shape (i.e. deviation from center over its timespan) between the BA/YD and other D-O events within the last 120,000 years, which leads us to question the uniqueness of the BA/YD in the Greenland record. Our approach is particularly novel for traditional paleoclimate research and we argue for the increased implementation of similarly robust statistical methods in paleoclimate research.

40 2 Methods

To study abrupt decadal-to-multidecadal changes in climate associated with each of the Dansgaard-Oeschger events, we examined published changes in oxygen isotope ratios ($\delta^{18}\text{O}$) and methane (CH_4) from the NGRIP Greenland ice cores (Rasmussen et al., 2014; Baumgartner et al., 2014) and $\delta^{18}\text{O}$ and carbon dioxide (CO_2) changes from the EDML, WAIS, Siple Dome, and TALDICE ice cores recovered from Antarctica (Barbante et al., 2006; Bereiter et al., 2015) that span the last 120,000 years
45 of Earth's climate history. For the purposes of our study, the timing of each Dansgaard-Oeschger event is taken from the ages published in the INTIMATE (INTEgration of Ice-core, MARine and TERrestrial records) dataset in Table 2 of Rasmussen et al. (2014). We then develop a stratigraphy that emphasizes the large-scale Dansgaard-Oeschger variability as follows: Firstly, as several interstadials in this record comprise of sub-events labeled by lowercase letters, for our work we consider these to be part of the larger interstadial, and not unique events. For example, while Greenland Interstadial 1 (i.e. the BA interstadial)
50 comprises of sub-events GI-1a through GI-1e, in our analysis this is simply treated as GI-1. A second set of sub-events in the INTIMATE dataset are also denoted by decimals in Rasmussen et al. (2014). For example, Dansgaard-Oeschger event 2 in the INTIMATE dataset is separated into two sub-events, labeled GS 2.1/GI2.1 and GS 2.2/GI 2.2. Due to their generally high amplitude and tendency to span multi-centennial timescales, these sub-events must at least initially be considered as Dansgaard-Oeschger ‘candidates’, and thus require a more rigorous procedure to be dealt with. Firstly, we consider cases when



55 two sub-events occur in succession and define a duration-based algorithm to determine whether each one should be considered a separate Dansgaard-Oeschger event, both combined into one single event, or omitted from our analysis entirely (Figure 2).

Of the eight Dansgaard-Oeschger events in this period containing two sub-events - namely numbers 2, 5, 15, 16, 17, 19, 21, and 23 - our main analysis, which is founded on conservative duration parameter choices ($x = 300$ yrs, $y = 300$ yrs, $z = 200$ yrs) leads to the selection of stadial and interstadials found in Table 1 (see columns 2-3 of Table 1 to observe how these choices differ under various parameter choices for x, y, z). Taking D-O event 2 as an example, we observe that GI2.2, GS2.2, and GI2.1 span 120, 200, and 120 years respectively, and thus the algorithm in Figure 2 leads to the combination of GI2.2, GS2.2, and GI2.1 into a single interstadial, since the sub-events are less than the parameter choices $x = 300, y = 300, z = 200$ respectively. In D-O event 5, however, GI5.2, GS5.2, and GI5.1 span 460, 1200, and 240 years, respectively, and thus under the same parameter choices, the interstadial-stadial choice algorithm in Figure 2 dictates that each sub-event should be treated as
65 its own stadial or interstadial. Note that our final results differ minimally based on how sub-cycles are chosen.

Beyond ~ 104 kyr BP, the CO_2 record contains only one datapoint for about every 500 years. Thus, to ensure the existence of a well-defined and complete record for all four of our chosen proxies, as we restrict our analysis of the last glacial cycle to the period of 104-11 kyr BP containing D-O events 1-23. Of the eight containing sub-events, our algorithm discards the second sub-event of four D-O events (i.e., 16.2, 17.2, 21.2, and 23.2), includes two second sub-events as distinct (i.e., 5.2 and 19.2),
70 absorbs GI15.1 into the sub-stadials surrounding it, and absorbs GS2.2 into the sub-interstadials surrounding it (see Table 1 for the algorithm's decisions for other parameter values). This amounts to the consideration of 25 D-O events, four of which are sub-events (i.e., events 5.1, 5.2, 19.1, and 19.2).

To initially examine the uniqueness of the pattern of climate change during Dansgaard-Oeschger event 1 (the BA/YD), we overlaid the NGRIP $\delta^{18}\text{O}$ record of each D-O event over the BA/YD. To facilitate the comparison of D-O cycles, we normalized
75 the timescale that covers each D-O event, as well as centered each record at its median. We then narrowed down the number of D-O events (including BA/YD) by visually selecting those events that most closely resembled the pattern of NGRIP $\delta^{18}\text{O}$ during the BA/YD.

To investigate more rigorously the shape (i.e. time evolving variability) of each of our chosen climate proxies (NGRIP $\delta^{18}\text{O}$, EDML $\delta^{18}\text{O}$, compiled Antarctic CO_2 , and NGRIP CH_4) during each Dansgaard-Oeschger event, including the BA/YD, we
80 calculated (i) the magnitude of change from interstadial to stadial (peak-to-trough analysis), (ii) the rate and direction (slope) of change of each proxy during each stadial, and (iii) the median value of each proxy during each stadial. In our peak-to-trough analysis, we derived a measure of the amplitude of change from the interstadial to the stadial by calculating the difference between the mean of the warmest interstadial points and the mean of the coldest stadial points for each D-O event in the NGRIP $\delta^{18}\text{O}$ record. To ensure that the peak interstadial warmth and maximum stadial cooling are selected, the mean values
85 are calculated using only the upper and lower 10% of the $\delta^{18}\text{O}$ values, respectively (Figure 3). We calculate this peak-to-trough measure for the other three proxies by taking the difference of the mean of its values within the time window of NGRIP $\delta^{18}\text{O}$'s maximum (minimum) 10% interstadial (stadial) values. For some proxies, where no data exists in a given short interstadial (stadial) time window, we take the maximum (minimum) of a 300 year moving gaussian filter (250yr for CO_2 , given sparsity of data at points), and while not ideal, it is the best approximation that our data limitations can offer.



90 We estimated the linear slope, and thus overall rate and direction of change, of each proxy during each of the stadials using ordinary least squares (OLS) regression. In many cases the NGRIP $\delta^{18}\text{O}$ record behavior during stadial periods is generally flat, so records with highly negative peak-to-trough measurements and stadial slopes close to zero are a good indicator of Dansgaard-Oeschger event behavior. Finally, the median of each proxy for each stadial in our analysis was calculated. The values of each of these metrics for each proxy across all 25 chosen D-O events are shown in Tables 2 and 3.

95 A robust principal component based outlier detection method, entitled PCOut, based on Filzmoser et al. (2008), was then applied to the results from our three metrics to test if the BA/YD is statistically different from other D-O events. This algorithm is proven to be efficient in high dimensions and especially effective in identifying location outliers, which is ideal for our data. We accept PCOut's slightly higher amount of false positives (i.e., higher size) than other algorithms on the basis that its extremely low level of false negatives (i.e., high power) is more important for this study since the areas in which the Younger
 100 Dryas is not unique is of particular interest. PCOut differs from typical principal component analysis schemes in two ways: 1) it robustly transforms the data before extracting principal components, and 2) it computes two measures of variance: one based on location and the other based on scatter. In short, PCOut first shifts an $n \times p$ data array by its variable-wise median and scales it by its variable-wise median absolute deviation (MAD), both of which are more robust (i.e., error resistant) estimators of location and scale (respectively) than sample mean and variance. In our case, we let $n = 25$ correspond to the number of D-O
 105 event observations, and let $p = 12$ variables denote the result of obtaining the three aforementioned metrics on each of the four proxies. PCOut then performs a standard principal component analysis (PCA) procedure to the transformed data that retains the first p^* components contributing 99% of the data's variance, and subsequently shifts and rescales the principal components once again by their new median and MAD. For an estimate of location exceptionality, PCOut is programmed to weight each of these remaining components z_{ij}^* by the following robust measure of kurtosis,

$$110 \quad w_j = \left| \frac{1}{n} \sum_{i=1}^n \frac{(z_{ij}^* - \text{med}(z_{1j}^*, \dots, z_{nj}^*))^4}{\text{MAD}(z_{1j}^*, \dots, z_{nj}^*)} - 3 \right| \text{ for } j = 1, \dots, p^* \quad (1)$$

and then computes a robust Euclidian distance RD_i for each of the n data points using these weights, where $W = \sum_{j=1}^{p^*} w_j$, the total weight, and the z_{ij}^* are the location shifted and rescaled principal components (visualized in panel 1, Figure 4):

$$RD_i = \sqrt{\sum_{j=1}^{p^*} \left(\frac{z_{ij}^* w_j}{W} \right)^2}. \quad (2)$$

This is followed by a further transformation to acquire the final robust distances d_i , where $\chi_{p^*,0.5}^2$ is the 50th percentile of a
 115 chi-squared distribution with p^* degrees of freedom:

$$d_i = RD_i \cdot \frac{\sqrt{\chi_{p^*,0.5}^2}}{\text{med}(RD_1, \dots, RD_n)}. \quad (3)$$



120 These d_i 's represent the degree of separation each of the n data points (corresponding to D-O cycles) experiences from the center of the data, where each RD_i is a robust calculation of the i th data vector's distance from its variable-wise median, and dividing by the median of the RD_i 's as in eq. 3 measures how much each RD_i deviates from the median of all such distances to produce d_i . To evaluate these distances as outliers or non-outliers, each data point is assigned a weight a_i based on its distance d_i such that higher distances receive a smaller weight so as to avoid outlier masking (visualized in panel 2, Figure 4):

$$a_i = \begin{cases} 0 & d_i \geq c \\ \left(1 - \left(\frac{d_i - M}{c - M}\right)^2\right)^2 & M < d_i < c \\ 1 & d_i \leq M \end{cases} \quad (4)$$

125 Finally, PCOut defines another metric b_i for each data point that uses the same exact procedure minus the kurtosis weighting step (i.e., unweighted euclidian distance $\sqrt{\sum_{j=1}^{p^*} \left(\frac{z_{ij}^*}{W}\right)^2}$ substitutes for eq. 2). For the a_i weight, the parameter M is the $\frac{1}{3}$ quantile of the distances $\{d_i\}$, and

$$c = \text{med}(d_1, \dots, d_n) + 2.5 \cdot \text{MAD}(d_1, \dots, d_n), \quad (5)$$

whereas the non-kurtosis weighted d_i are proven to follow $\chi_{p^*}^2$ relatively closely, so $(M^2, c^2) = (\chi_{p^*, .25}^*, \chi_{p^*, .99}^*)$ in eq. 4's calculation of b_i . In the final test (visualized in panel 3, Figure 4), outliers are then defined as data points where

$$\frac{(a_i + 0.25)(b_i + 0.25)}{(1.25)^2} < 0.25. \quad (6)$$

130 PCOut achieves much higher precision than a traditional principal component analysis scheme because of the strategic weighting mechanisms aimed to iteratively reduce the degree which outliers mask their own presence (Filzmoser et al., 2008). Further, its use of robust statistical estimators suits our constructed dataset well in that the metrics calculated are subject to high uncertainty. For a graphical representation of PCOut's data transformations spanning eq.'s 2-6, see Figure 4.

135 PCOut is not applicable to single variable data because principal component analysis is not a valid procedure for $p = 1$, so outliers in this case are determined using a simpler criterion: if some data point $x_i \notin [Q_1 - \text{MAD}(x_1, \dots, x_n), Q_3 + \text{MAD}(x_1, \dots, x_n)]$, where Q_1, Q_3 are the first and third quantiles of the data, respectively, it is considered an outlier.

3 Results

140 To understand the BA/YA's behavior with respect to the other 24 D-O events under consideration in this study, we first find seven other D-O events (namely events 7, 8, 11, 12, 13, 16, and 19.2) whose shape in the NGRIP $\delta^{18}\text{O}$ record bears remarkable similarity to BA/YD when the time from interstadial to stadial is normalized (Figure 5). Furthermore, the overlay of mean behavior of all D-O events excluding the BA/YA corroborates that this period is also strikingly similar in NGRIP $\delta^{18}\text{O}$ shape to the average D-O event in the entire period, as shown by the mean line plotted in Figure 5.



145 These overlays are also completed for the other three proxies (i.e. CH₄ from Greenland, compiled CO₂ from Antarctic, and δ¹⁸O from EDML). Beginning with NGRIP CH₄, Figure 5 indicates no clear overall pattern to the D-O time series, as the mean line is nearly flat. This confirms a similar lack of uniqueness in BA/YD's CH₄ proxy, which our PCOut analysis will later confirm. The BA/YD appears not to strictly follow the trend of the seven time series lines or mean line in the two Antarctic proxy overlays (EDML δ¹⁸O and CO₂), which indicates that further study is required to determine how the BA/YD might constitute an exceptional event from the perspective of proxies in the Southern Hemisphere.

150 The results from our PCOut analysis allows for additional categorization of the Younger Dryas either as outlier or non-outlier in all variable subsets when equipped with our three metrics applied to four different chemical proxies for all 25 D-O cycles under consideration. The rationale for observing the Younger Dryas' outlier behavior in all subsets of the 12-variable system is to understand how chemical makeup (NGRIP δ¹⁸O, NGRIP CH₄, EDML δ¹⁸O, compiled Antarctic CO₂), proxy shape (peak-to-trough, stadial slope), and proxy location (median), might individually render this period unique (or not unique). Given PCOut's low level of false negatives compared to other tests of its kind, we take non-outlier results seriously as indicators that
155 Younger Dryas is not statistically exceptional as a D-O event. Our results pertaining to the BA/YD are summarized in Table 4, which indicates the subsets of proxies and metrics for which the BA/YD is an outlier or not - "YES" ("NO") means that the BA/YA is (not) an outlier within that subset.

Beginning with single variable results, we find that all but two cells in the median column (column 7) of Table 4 exhibit outlier behavior. This result is unsurprising given that the BA/YD occurs during a period of overall warming closer to the
160 Holocene and thus higher percentages of all chemical proxies compared to other D-O events, which all occurred during the coldest stretches of the past 120 kyr. Median measurements for other D-O cycles on the edges of the last glacial period also harbor a proportionally higher level of median measurements due to their temporal proximity to warmer periods before and after the last glacial period. In fact, we find that the set of median-only PCOut results for D-O events 2, 20, and 23 harbor 47%, 60%, and 53% outliers, respectively, which indicates that we can consistently expect subsets of measurements including the
165 median to be greater for D-O events near the beginning and end of the last glacial period. Thus, we attribute the a portion of the BA/YD's outlier behavior in variable subsets including the median to a known temperature increase during the time of its occurrence.

In the single variable stadial slope column (column 6, Table 4), we find particular interest in the fact that all proxy pairs including NGRIP δ¹⁸O (rows 6-8) do not register as outliers, while all proxy pairs not including NGRIP δ¹⁸O (rows 9-11) do
170 register as outliers. This exact phenomenon is also reflected in the paired peak-to-peak and stadial slope column (column 2, Table 4), strongly indicating that the presence of NGRIP δ¹⁸O within a given variable subset is associated with a lack of outlier behavior of the shape of the BA/YA. The other two pairs of metrics (columns 3-4, Table 4) exhibit no clear pattern, although it should be noted that the single and paired Greenland proxies (rows 8, 12, and 15) register as outliers in only one of their cells.

175 It must be noted that 80% of proxy subsets in the first (all-metric) column of Table 4 register as outliers within their distribution. While this result should be taken with skepticism due to the inclusion of the median, which has been seen to contribute significantly to outlier behavior in numerous other cases, it should not be ignored that the BA/YD is an outlier under all of our metrics and proxies combined.



Our main goal is to assess the exceptionality of the BA/YA in the Greenland proxy record. While the single proxy NGRIP $\delta^{18}\text{O}$ section (row 12, Table 4) exhibits a mix of measured outliers and non-outliers, it must be taken into account that all variable subsets in this row that cause the BA/YD to become an outlier contain the median measurement, which, as previously stated, contributes significantly to the BA/YD's outlier behavior due to known warming leading up to the Holocene.

The single proxy NGRIP CH_4 row (Table 4) exhibits no outlier behavior whatsoever across all variable subsets. This record generally follows the shape of its NGRIP $\delta^{18}\text{O}$ counterpart, yet often seems to lag or lead $\delta^{18}\text{O}$ by centennial timescales (Baumgartner et al., 2012), inevitably causing higher variance in shape metrics chosen in this study. So, a lack of outlier behavior across all NGRIP CH_4 subsets primarily indicates that Younger Dryas' lag in CH_4 is not unusual. This lack in the NGRIP CH_4 single variable median category is also somewhat surprising, and suggests that the magnitude of CH_4 amongst all D-O cycles is less closely tied to glacial-interglacial cycles than NGRIP $\delta^{18}\text{O}$.

Observing the two NGRIP ($\delta^{18}\text{O}$, CH_4) records paired across all metric subsets (row 8, Table 4) leads to further interest: namely, no outlier behavior in metrics other than the pure median exists. Since much of the ice-core based knowledge generated on the Younger Dryas relies on these two cores, a lack of outlier behavior in shape is a major result, and confirms our analysis of Figure 5. We observe this in the scatterplots of Figure 6, which plot the value of pairs of metrics for the Greenland shape measurements across all 25 D-O events, and clearly indicate that for each such pair, the BA/YA is within the natural scatter range of all other D-O events. In particular, notice that for the paired peak-to-trough scatterplots (third panel down from first column of Figure 6), the distribution of points roughly forms a ring of which BA/YA is a part, since there is always at least one other point in the plot that is more outlying in either direction. Similarly, in the paired slope scatterplots (fourth panel down from second column of Figure 6), the distribution of points forms a roughly straight line of which the BA/YA is also a part. In fact, these plots provide an excellent example of what an outlier would look like, namely, the point far to the far right of all others in this plot, which turns out to be D-O 23. In sum, if the shape of the BA/YD were an outlier in the Greenland record, these scatter plots would display a clear separation of the BA/YD from all other points in the scatter.

Note that we use the stadial/interstadial length parameters $(x, y, z) = (300, 300, 200)$ to choose 25 D-O cycles for this section, but different parameter choices that output 28-30 D-O cycles for analysis (see Table 1) yield results that are 86-93% similar across all D-O cycles.

4 Discussion

The aim of this study is to precisely and robustly classify the proxy-based qualities that would render the BA/YA a unique climate event in the context of other abrupt episodes of climate change during the last 120,000 years, known as Dansgaard-Oeschger events. If the BA/YD is to be excluded from the list of D-O events, or assigned its own particular set of triggering mechanisms there must be some statistically sound reason for doing so.

Using four chemical proxies commonly included in assessments of general D-O behavior - $\delta^{18}\text{O}$ and CH_4 from NGRIP, Greenland, $\delta^{18}\text{O}$ from EDML, Antarctica, and compiled CO_2 from multiple Antarctic records - we refrain from performing traditional cross correlation analysis to test for lags, and instead employ a more holistic approach that captures the shape of



each D-O cycle in terms of multiple variables. Three measurements to characterize both the location (median) and shape (peak-to-trough difference, stadial slope) of each chemical proxy for each D-O cycle are taken, and inputted into a robust principal component analysis algorithm (PCOut) to test for outliers.

Our main result is as follows: the BA/YD is not a unique event with respect to the other D-O events recorded in the Greenland ice core record, other than the fact that its median $\delta^{18}\text{O}$ levels are higher due to its proximity to deglacial warming into the Holocene. The increase in median $\delta^{18}\text{O}$ is also not unique to the BA/YA, as D-O events 2, 20, and 23 exhibit a similar phenomenon, which we attribute to their occurrence proximal to long term global climate fluctuations. The non-uniqueness of the BA/YD's shape is clearly indicated by the statistical indistinguishability of the changes in the Greenland ice core record with the other D-O events, especially in terms of its $\delta^{18}\text{O}$ variability, for which one-third of other D-O events appear virtually identical (Figure 5). Thus, the BA/YD period cannot and should not be distinguished from any other D-O cycle in the last glacial period on the basis of Greenland ice core time series shape. In this context, the BA/YD should be understood as a classic example of a D-O event, and deserves further consideration as such when studying the mechanisms that triggered it. The hypothesized meltwater forcing mechanism commonly invoked for the BA/YA is seldom considered for the other D-O events, and visa versa, the major triggering mechanisms for the D-O events are rarely used to explain the BA/YD. Our results suggest that understanding the causes of the BA/YD would benefit from examining the mechanisms used to explain D-O events, rather than relying overwhelmingly on the meltwater hypothesis. Indeed, the role of meltwater forcing in triggering the YD has been questioned a number of times since it was first proposed by W. Broecker and others in 1989. For instance, the YD is widely viewed as a time of glacial re-advance and reduced terrestrial meltwater discharge to the ocean, such that it is likely that freshwater forcing was less during this period (Abdul et al., 2016), making it difficult to explain how the overturning circulation remained weakened for the 1000 year duration of the YD stadial (Renssen et al., 2015). In addition, the termination of the YD, and subsequent rapid warming into the Holocene coincide with a time of increasing meltwater runoff to the North Atlantic (e.g. Fairbanks (1989)) as the Laurentide Ice sheet over North America finally collapsed.

Data availability. Measurement for this project can be found in Tables 2 and 3.

Author contributions. Author 1 conducted all data analysis, figure creation, and manuscript drafting. Author 2 advised throughout the research process and edited manuscript as necessary.

Competing interests. The authors declare that they have no conflict of interest.

<https://doi.org/10.5194/cp-2020-43>
Preprint. Discussion started: 7 April 2020
© Author(s) 2020. CC BY 4.0 License.



Acknowledgements. This study is made possible by the Summer Student Fellow Program at Woods Hole Oceanographic Institution as well as NSF REU OCE-1852460. Special thanks to Carl Wunsch, Olivier Marchal, and Andy Solow for extra advising.



References

- 240 Abdul, N. A., Mortlock, R. A., Wright, J. D., and Fairbanks, R. G.: Younger Dryas sea level and meltwater pulse 1B recorded in Barbados reef crest coral *Acropora palmata*, *Paleoceanography*, 31, 330–344, <https://doi.org/10.1002/2015PA002847>, 2016.
- Baldini, J. U. L., Brown, R. J., and Mawdsley, N.: Evaluating the link between the sulfur-rich Laacher See volcanic eruption and the Younger Dryas climate anomaly, *Climate of the Past*, 14, 969–990, <https://doi.org/10.5194/cp-14-969-2018>, 2018.
- Barbante, C., Barnola, J.-M., Becagli, S., Beer, J., Bigler, M., Boutron, C., Blunier, T., Castellano, E., Cattani, O., Chappellaz, J., Dahl-
245 Jensen, D., Debret, M., Delmonte, B., Dick, D., Falourd, S., Faria, S., Federer, U., Fischer, H., Freitag, J., Frenzel, A., Fritzsche, D., Fundel, F., Gabrielli, P., Gaspari, V., Gersonde, R., Graf, W., Grigoriev, D., Hamann, I., Hansson, M., Hoffmann, G., Hutterli, M. A., Huybrechts, P., Isaksson, E., Johnsen, S., Jouzel, J., Kaczmarek, M., Karlin, T., Kaufmann, P., Kipfstuhl, S., Kohno, M., Lambert, F., Lambrecht, A., Lambrecht, A., Landais, A., Lawer, G., Leuenberger, M., Littot, G., Loulergue, L., Lüthi, D., Maggi, V., Marino, F., Masson-Delmotte, V., Meyer, H., Miller, H., Mulvaney, R., Narcisi, B., Oerlemans, J., Oerter, H., Parrenin, F., Petit, J.-R., Raisbeck, G.,
250 Raynaud, D., Rothlisberger, R., Ruth, U., Rybak, O., Severi, M., Schmitt, J., Schwander, J., Siegenthaler, U., Siggaard-Andersen, M.-L., Spahni, R., Steffensen, J. P., Stenni, B., Stocker, T. F., Tison, J.-L., Traversi, R., Udisti, R., Valero-Delgado, F., van den Broeke, M. R., van de Wal, R. S. W., Wagenbach, D., Wegner, A., Weiler, K., Wilhelms, F., Winther, J.-G., Wolff, E., and Members, E. C.: One-to-one coupling of glacial climate variability in Greenland and Antarctica, *Nature*, 444, 195–198, <https://doi.org/10.1038/nature05301>, 2006.
- Baumgartner, M., Schilt, A., Eicher, O., Schmitt, J., Schwander, J., Spahni, R., Fischer, H., and Stocker, T.: High-resolution inter-polar
255 difference of atmospheric methane around the Last Glacial Maximum, *Biogeosciences*, 9, 3961–3977, <https://doi.org/10.5194/bg-9-3961-2012>, 2012.
- Baumgartner, M., Kindler, P., Eicher, O., Floch, G., Schilt, A., Schwander, J., Spahni, R., Capron, E., Chappellaz, J., Leuenberger, M., Fischer, H., and Stocker, T. F.: NGRIP CH₄ concentration from 120 to 10 kyr before present and its relation to a $\delta^{15}\text{N}$ temperature reconstruction from the same ice core, *Climate of the Past*, 10, 903–920, <https://doi.org/10.5194/cp-10-903-2014>, 2014.
- 260 Bereiter, B., Eggleston, S., Schmitt, J., Nehrbass-Ahles, C., Stocker, T. F., Fischer, H., Kipfstuhl, S., and Chappellaz, J.: Revision of the EPICA Dome C CO₂ record and 800 and 600 kyr before present, *Geophysical Research Letters*, 42, 542–549, <https://doi.org/10.1002/2014GL061957>, 2015.
- Broecker, W. S., Peteet, D. M., and Rind, D.: Does the ocean-atmosphere system have more than one stable mode of operation?, *Nature*, 315, 21–26, <https://doi.org/10.1038/315021a0>, 1985.
- 265 Broecker, W. S., Kennett, J. P., Flower, B. P., Teller, J. T., Trumbore, S., Bonani, G., and Wolfl, W.: Routing of meltwater from the Laurentide Ice Sheet during the Younger Dryas cold episode, *Nature*, 341, 318–321, <https://doi.org/10.1038/341318a0>, 1989.
- Clark, P. U., Marshall, S. J., Clarke, G. K. C., Hostetler, S. W., Licciardi, J. M., and Teller, J. T.: Freshwater Forcing of Abrupt Climate Change During the Last Glaciation, *Science*, 293, 283–287, <https://doi.org/10.1126/science.1062517>, 2001.
- Dansgaard, W.: Greenland Ice Core Studies, *Palaeogeography, Palaeoclimatology, Palaeoecology*, 50, 185–187, 1985.
- 270 Fairbanks, R. G.: A 17,000-year glacio-eustatic sea level record: influence of glacial melting rates on the Younger Dryas event and deep-ocean circulation, *Nature*, 342, 637–642, 1989.
- Filzmoser, P., Maronna, R., and Werner, M.: Outlier identification in high dimensions, *Computational Statistics and Data Analysis*, 52, 1694–1711, <https://doi.org/10.1016/j.csda.2007.05.018>, 2008.
- Firestone, R. B., West, A., Kennett, J. P., Becker, L., Bunch, T. E., Revay, Z. S., Schultz, P. H., Belgia, T., Kennett, D. J., Erlandson, J. M.,
275 Dickenson, O. J., Goodyear, A. C., Harris, R. S., Howard, G. A., Kloosterman, J. B., Lechler, P., Mayewski, P. A., Montgomery, J., Poreda,



- R., Darrah, T., Hee, S. S. Q., Smith, A. R., Stich, A., Topping, W., Wittke, J. H., and Wolbach, W. S.: Evidence for an extraterrestrial impact 12,900 years ago that contributed to the megafaunal extinctions and the Younger Dryas cooling, *Proceedings of the National Academy of Sciences*, 104, 16016–16021, <https://doi.org/10.1073/pnas.0706977104>, 2007.
- 280 Keigwin, L. D., Klotsko, S., Zhao, N., Reilly, B., Giosan, L., and Driscoll, N. W.: Deglacial floods in the Beaufort Sea preceded Younger Dryas cooling, *Nature Geoscience*, 11, 599–604, <https://doi.org/10.1038/s41561-018-0169-6>, 2018.
- Li, C. and Born, A.: Coupled atmosphere-ice-ocean dynamics in Dansgaard-Oeschger events, *Quaternary Science Reviews*, 203, 1 – 20, <https://doi.org/10.1016/j.quascirev.2018.10.031>, 2019.
- Lohmann, J. and Ditlevsen, P. D.: Random and externally controlled occurrences of Dansgaard–Oeschger events, *Climate of the Past*, 14, 609–617, <https://doi.org/10.5194/cp-14-609-2018>, 2018.
- 285 Lohmann, J. and Ditlevsen, P. D.: Objective extraction and analysis of statistical features of Dansgaard–Oeschger events, *Climate of the Past*, 15, 1771–1792, <https://doi.org/10.5194/cp-15-1771-2019>, 2019.
- Rasmussen, S. O., Bigler, M., Blockley, S. P., Blunier, T., Buchardt, S. L., Clausen, H. B., Cvijanovic, I., Dahl-Jensen, D., Johnsen, S. J., Fischer, H., Gkinis, V., Guillevic, M., Hoek, W. Z., Lowe, J. J., Pedro, J. B., Popp, T., Seierstad, I. K., Steffensen, J. P., Svensson, A. M., Vallelonga, P., Vinther, B. M., Walker, M. J., Wheatley, J. J., and Winstrup, M.: A stratigraphic framework for abrupt climatic changes 290 during the Last Glacial period based on three synchronized Greenland ice-core records: refining and extending the INTIMATE event stratigraphy, *Quaternary Science Reviews*, 106, 14 – 28, <https://doi.org/10.1016/j.quascirev.2014.09.007>, 2014.
- Renssen, H., Mairesse, A., Goosse, H., Mathiot, P., Heiri, O., Roche, D., Nisancioglu, K., and Valdes, P.: Multiple causes of the Younger Dryas cold period, *Nature Geoscience*, <https://doi.org/10.1038/ngeo2557>, 2015.

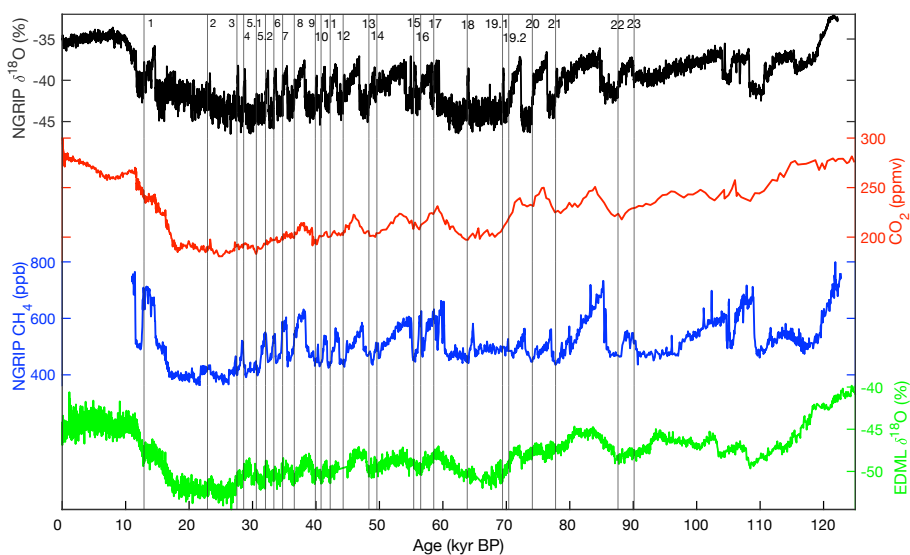


Figure 1. Full time series of all four proxies used. From top down: NGRIP $\delta^{18}\text{O}$, compiled CO_2 from EDML, WAIS, Siple Dome, and TALDICE, NGRIP CH_4 , and EDMIL $\delta^{18}\text{O}$. Vertical lines indicate the main 25 interstadial-to-stadial transitions used in this study, labeled by number from Rasmussen et al. (2014).

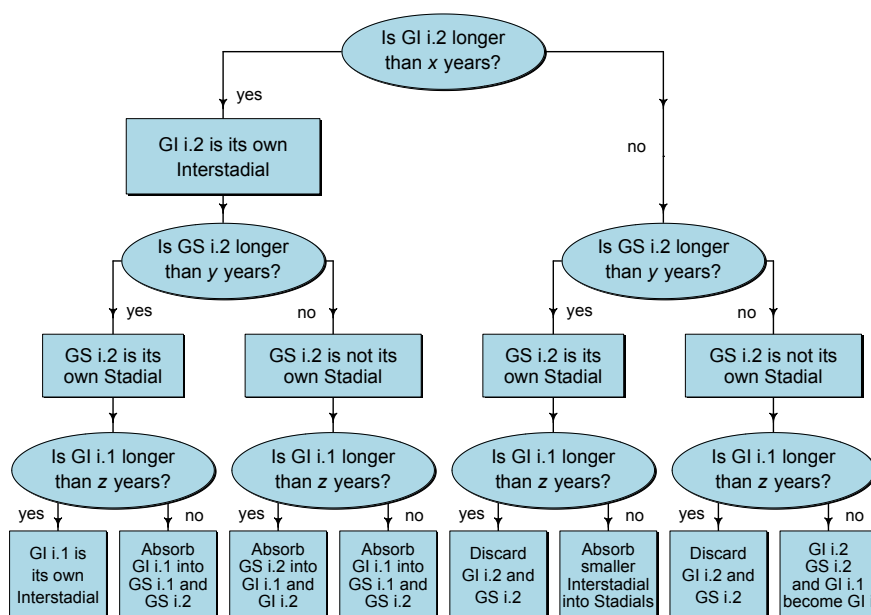


Figure 2. Duration-based scheme for including D-O cycles in analysis. Given the variety of climatic shifts present in the high-resolution INTIMATE NGRIP $\delta^{18}\text{O}$ stratigraphy, it is necessary to form a rigorous criterion for choosing D-O events to analyze. Since the duration of each D-O event in the INTIMATE stratigraphy is directly tied to the confidence that it exhibit the true characteristics of a D-O interstadial (stadial) period, we employ the above decision tree for determining which warm/cold couples split up by the INTIMATE stratigraphy can confidently be considered their own unique D-O events with flexible duration parameters (x, y, z) .

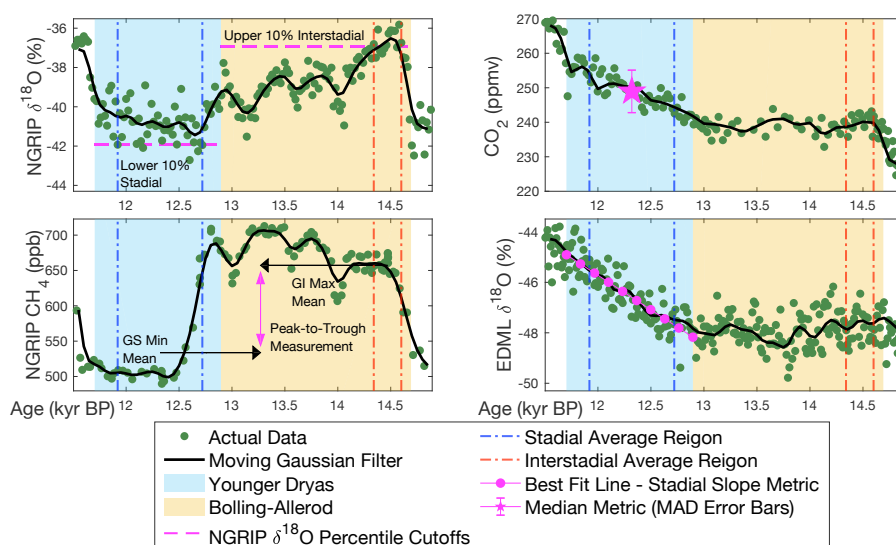


Figure 3. Three Metrics for capturing the shape and location of D-O cycles across multiple chemical proxies. In all panels, raw data is presented in green, while interpolated data using a 300yr moving gaussian filter (250yr for CO_2 , given sparsity of data at points) is presented in black. Blue and orange background shading represents stadal and interstadial conditions, respectively, while pink overlays exemplify the three measurements taken: in the NGRIP $\delta^{18}\text{O}$ panel (upper left), the extreme 10% percentiles of the $\delta^{18}\text{O}$ data are determined, and the time window into which all such data falls are extracted (blue (Stadal) and red (Interstadial) vertical average regions). The difference in means of each proxy's data within these time windows for any given D-O cycle constitutes that proxy's peak-to-trough (labeled peak-to-peak) measurement (shown in lower left NGRIP CH_4 panel). The OLS linear slope of the stadal data estimates determine the stadal slope for each proxy in each D-O cycle (shown in the lower right EDML $\delta^{18}\text{O}$ panel). The third and final metric measured is the stadal median (shown in the upper right panel). Despite each panel only displaying one metric, note that all are applied to all four proxies and all D-O events.

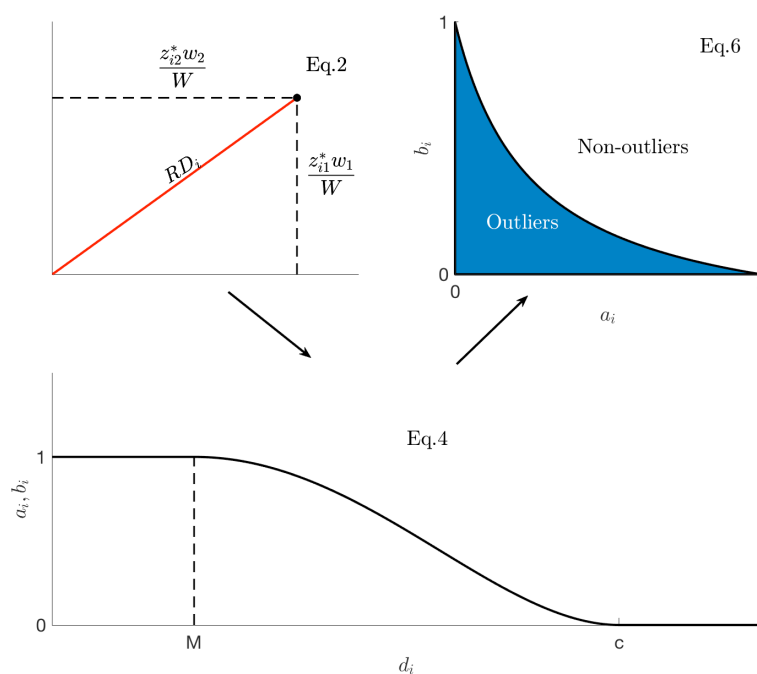


Figure 4. PCOut’s main outlier decision steps. After completing PCA to produce centered and rescaled components z_{ij}^* , eq. 2 calculates the “distance” RD_i of the i th component vector from zero with sums of squares (panel 1). After rescaling the RD_i ’s to create new “distances” d_i , we calculate quantities a_i, b_i based on the function in panel 2 (eq. 4), such that large distances d_i translate into smaller values of a_i, b_i . Finally, panel 3 illustrates the region by which PCOut classifies a_i, b_i as indicative of the i th datapoint being an outlier or not (eq. 6).

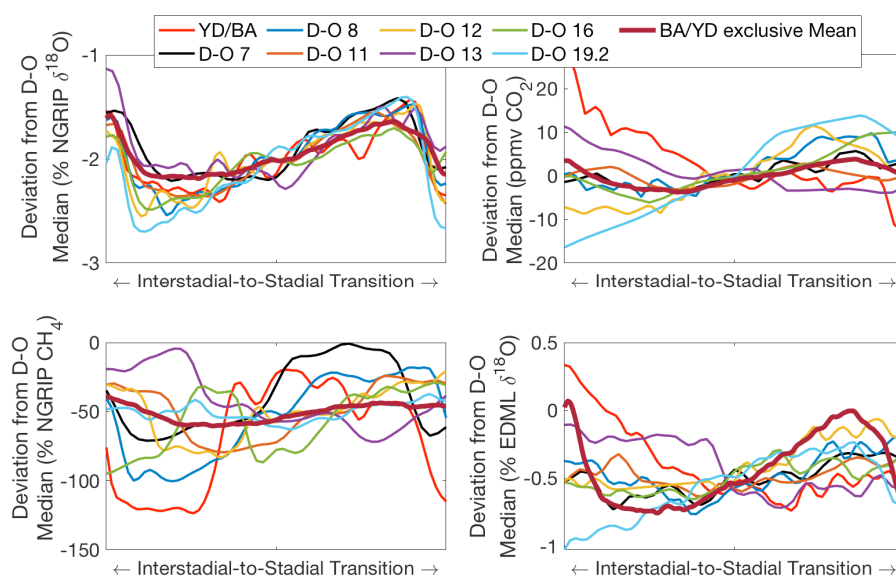


Figure 5. Shapes of eight D-O events and grand mean (excluding the BA/YD) with respect to all four proxies. Representing one-third of D-O events during the last glacial period, these D-O events' respective NGRIP $\delta^{18}O$ records bear remarkable similarity to that of the BA/YD, despite assumptions of its uniqueness. Additionally, the BA/YD exclusive mean of D-O events' NGRIP $\delta^{18}O$ record confirms that the shape of the BA/YD does not visibly deviate from the classic D-O shape. Further, Antarctic records (CO_2 and EDML $\delta^{18}O$, second column) show varying trends that do not appear particularly synchronized to the D-O sawtooth shape. NGRIP CH_4 exhibits D-O-like variability, with varying leads and lags.

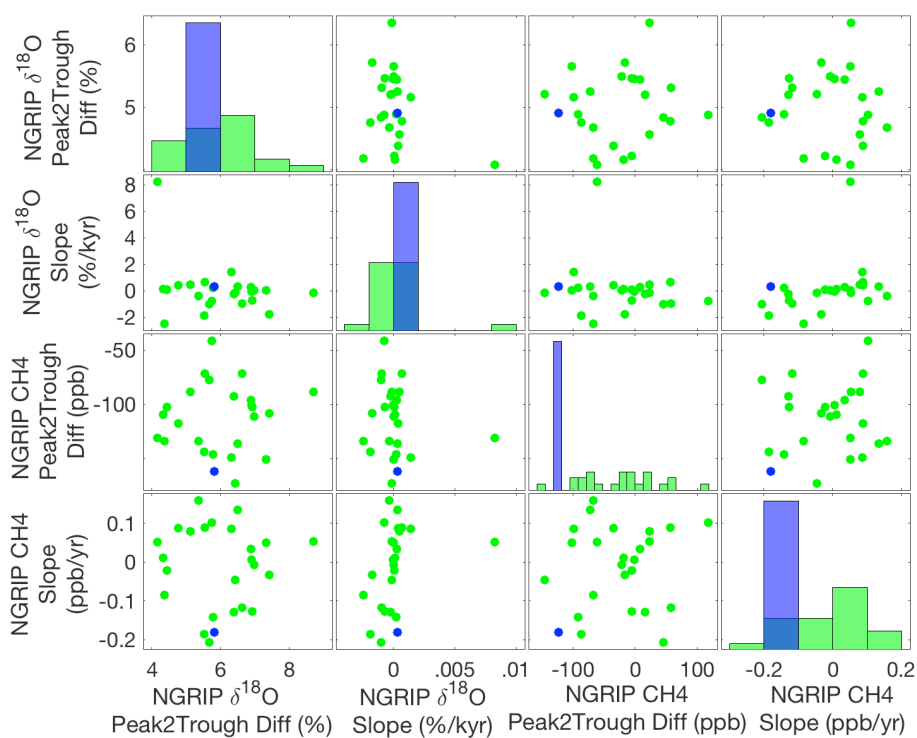


Figure 6. Greenland shape scatter grid. Of the 105 multivariate subsets analyzed for outliers, the above represents the essence of our results. Using both peak-to-trough stadial slope and measurements of NGRIP $\delta^{18}\text{O}$ and CH_4 (left), we observe minimal outlier behavior from the YD in each pair of the four variable system, which indicates that the shape of the YD's Greenland proxy records is not unique in of itself. Histograms along the diagonal plot the corresponding single-variable distribution, where the horizontal location of the YD's measurement is in purple on a normalized scale (i.e., the height of the purple bar is 1).



Table 1. Three difference stadial choice situations for different duration parameter choices in Figure 2. The choice results in the first column $((x, y, z) = (300, 300, 200))$ represent our main point of departure for statistical analysis. Note that basing analysis on the stratigraphic choices represented in the second or third columns yields 86-93% similarity in results.

Decision Tree Results

Cycle #	Threshold		
	$(x, y, z) = (300, 300, 200)$	$(x, y, z) = (90, 100, 140)$	$(x, y, z) = (90, 100, 90)$
2	Join GI2.1,2.2, and GS2.2 into GI2	Absorb GI2.1 into GS2.1,2.2	Treat cycles 2.1 and 2.2 as separate
5	Treat cycles 5.1 and 5.2 as separate	Treat cycles 5.1 and 5.2 as separate	Treat cycles 5.1 and 5.2 as separate
15	Absorb GI15.1 into GS15.1,15.2	Absorb GI15.1 into GS15.1,15.2	Treat cycles 15.1 and 15.2 as separate
16	Discard cycle 16.2	Treat cycles 16.1 and 16.2 as separate	Treat cycles 16.1 and 16.2 as separate
17	Discard cycle 17.2	Treat cycles 17.1 and 17.2 as separate	Treat cycles 17.1 and 17.2 as separate
19	Treat cycles 19.1 and 19.2 as separate	Treat cycles 19.1 and 19.2 as separate	Treat cycles 19.1 and 19.2 as separate
21	Discard cycle 21.2	Treat cycles 21.1 and 21.2 as separate	Treat cycles 21.1 and 21.2 as separate
23	Discard cycle 23.2	Treat cycles 23.1 and 23.2 as separate	Treat cycles 23.1 and 23.2 as separate



Table 2. Metric measurements for Greenland proxies. Abbreviations for proxies are given by $\delta^{18}\text{O}$ =NGRIP $\delta^{18}\text{O}$ and CH_4 =NGRIP CH_4 , and abbreviations for metrics are given by P2T=peak-to-trough, Slp=stadial slope, and Med=median.

D-O #	$\delta^{18}\text{O}$ P2T	$\delta^{18}\text{O}$ Slp	$\delta^{18}\text{O}$ Med	CH_4 P2T	CH_4 Slp	CH_4 Med
1	5.82	0.000341	-40.73	-123.59	-0.181	509.80
2	4.33	0.000126	-41.99	-18.27	0.011	404.95
3	6.98	0.000011	-43.47	-22.04	-0.008	400.45
4	6.63	-0.000958	-43.95	56.95	-0.118	470.40
5.1	4.43	0.000090	-44.28	-5.33	-0.022	419.00
5.2	6.39	-0.000228	-43.69	15.37	-0.129	475.40
6	6.93	-0.000713	-43.81	-5.13	-0.128	467.80
7	5.78	0.000224	-42.71	-91.68	-0.143	467.60
8	6.42	-0.000144	-43.02	-145.68	-0.046	458.80
9	5.12	0.000470	-43.08	22.96	0.079	481.20
10	6.31	0.001404	-42.50	-98.50	0.086	457.80
11	5.36	-0.000372	-42.29	-67.87	0.158	510.50
12	6.5	0.000328	-42.68	-72.63	0.134	516.20
13	5.55	0.000660	-42.87	56.47	0.089	532.20
14	4.36	-0.002479	-41.52	-67.58	-0.086	486.55
15	5.75	-0.000763	-42.52	117.16	0.102	581.90
16	5.52	-0.001892	-42.29	-87.00	-0.185	574.70
17	5.67	-0.001038	-42.04	45.40	-0.207	610.10
18	6.89	0.000264	-43.65	7.79	0.034	474.00
19.1	6.9	-0.000041	-43.87	-1.60	0.005	490.50
19.2	7.43	-0.001761	-43.96	-16.95	-0.033	496.75
20	8.71	-0.000154	-44.50	23.18	0.054	519.05
21	7.32	0.000036	-42.59	-101.45	0.051	515.15
22	4.76	0.000397	-41.20	-34.71	0.088	489.90
23	4.16	0.008229	-39.93	-61.53	0.051	512.05



Table 3. Metric measurements for Antarctic proxies. Abbreviations for proxies are given by EDML=EDML $\delta^{18}\text{O}$ and compiled Antarctic $\text{CO}_2 = \text{CO}_2$, and abbreviations for metrics are given by P2T=peak-to-trough, Slp=stadial slope, and Med=median.

D-O #	EDML P2T	EDML Slp	EDML Med	CO_2 P2T	CO_2 Slp	CO_2 Med
1	1.12	0.002738	-46.46	9.12	0.0123	248.95
2	0.22	0.000534	-51.40	8.10	0.0069	202.93
3	-1.58	-0.000035	-52.22	-6.07	-0.0006	186.14
4	-0.85	-0.00087	-50.96	-3.08	-0.0032	189.65
5.1	0.65	0.000850	-50.19	5.90	0.0044	189.83
5.2	-1.17	-0.000367	-50.96	-5.08	-0.0072	191.23
6	-0.49	-0.000420	-50.50	-0.63	-0.0050	196.14
7	-1.19	-0.000516	-50.78	-7.88	-0.0040	196.07
8	-1.02	0.001384	-50.20	-11.34	0.0011	201.78
9	1.15	0.001336	-49.17	11.65	0.0072	206.09
10	-0.42	0.000794	-50.23	-3.42	-0.0202	197.90
11	-0.44	0.001256	-50.08	-3.21	0.0191	201.12
12	-1.61	-0.000310	-49.54	-15.20	-0.0003	202.59
13	0.92	0.001278	-48.25	3.75	0.0043	206.18
14	-1.02	-0.000076	-49.60	-19.76	-0.0247	202.09
15	0.31	0.000001	-48.93	1.46	0.0085	215.38
16	-0.83	0.000161	-49.64	-13.45	0.0079	208.97
17	-0.54	-0.001232	-48.54	-6.58	-0.0038	223.15
18	0.58	0.000539	-49.26	8.49	0.0060	210.57
19.1	-0.53	-0.000012	-50.66	-7.24	-0.0005	202.55
19.2	-2.28	-0.001508	-49.55	-28.21	-0.0093	213.41
20	-0.08	-0.000665	-48.16	-13.03	0.0002	232.54
21	-2.02	-0.000500	-47.44	-8.19	0.0141	231.68
22	0.23	0.000969	-47.17	-3.73	0.0083	226.07
23	-1.11	-0.000438	-47.98	-13.36	0.0000	229.33



Table 4. PCOut BA/YD Results. “YES” (“NO”) indicates that the BA/YD is (not) an outlier in the subset indicated by the row/column combination in which it’s located. Rows refer to the prox(ies) under analysis ($\delta^{18}\text{O}$ = NGRIP $\delta^{18}\text{O}$, compiled Antarctic $\text{CO}_2 = \text{CO}_2$, EDML= EDML $\delta^{18}\text{O}$, and $\text{CH}_4 = \text{NGRIP CH}_4$), and columns refers to the metric(s) applied to those proxies (P2T=peak-to-trough, Slp=stadial slope, and Med= median). This amounts to an $n \times p$ -variate input into PCOut, where n denotes the number of proxies included and p denotes the metrics applied to all such proxies.

		1	2	3	4	5	6	7
		(P2T,Slp,Med)	(P2T,Slp)	(Slp,Med)	(P2T,Med)	(P2T)	(Slp)	(Med)
1	($\delta^{18}\text{O}, \text{CO}_2, \text{EDML}, \text{CH}_4$)	YES	YES	YES	YES	NO	YES	NO
2	($\delta^{18}\text{O}, \text{CO}_2, \text{EDML}$)	YES	NO	YES	NO	NO	NO	YES
3	($\delta^{18}\text{O}, \text{CO}_2, \text{CH}_4$)	YES	NO	YES	YES	YES	NO	YES
4	($\text{CO}_2, \text{EDML}, \text{CH}_4$)	YES	YES	YES	NO	YES	YES	YES
5	($\delta^{18}\text{O}, \text{EDML}, \text{CH}_4$)	NO	YES	NO	YES	YES	YES	YES
6	($\delta^{18}\text{O}, \text{CO}_2$)	YES	NO	YES	YES	NO	NO	YES
7	($\delta^{18}\text{O}, \text{EDML}$)	YES	NO	NO	YES	YES	NO	YES
8	($\delta^{18}\text{O}, \text{CH}_4$)	NO	NO	NO	NO	NO	NO	YES
9	(CO_2, EDML)	YES	YES	YES	YES	NO	YES	YES
10	(CO_2, CH_4)	YES	YES	YES	YES	NO	YES	YES
11	(EDML, CH_4)	YES	YES	YES	NO	YES	YES	YES
12	($\delta^{18}\text{O}$)	YES	NO	NO	YES	NO	NO	YES
13	(CO_2)	YES	NO	YES	YES	NO	NO	YES
14	(EDML)	YES	YES	YES	YES	NO	YES	YES
15	(CH_4)	NO	NO	NO	NO	NO	NO	NO